PNAS RESEARCH ARTICLE | BIOPHYSICS AND COMPUTATIONAL BIOLOGY

Scaling the glassy dynamics of active particles: Tunable fragility and reentrance

Puneet Pareek[a], Peter Sollich[b], Saroj Kumar Nandi[a,1], and Ludovic Berthier[c]

Edited by Michael Cates, University of Cambridge, Cambridge, United Kingdom; received June 24, 2025; accepted November 25, 2025

Understanding the influence of activity on dense amorphous assemblies is crucial for biological processes such as wound healing, embryogenesis, or cancer progression. Here, we study the effect of self-propulsion forces of amplitude f_0 and persistence time τ_p in dense assemblies of soft repulsive particles by simulating a model particle system that interpolates between particulate active matter and biological tissues. We identify the fluid and glass phases of the three-dimensional phase diagram obtained by varying f_0, τ_p, and the packing fraction ϕ. The morphology of the phase diagram accounts for a nonmonotonic evolution of the relaxation time with τ_p, which is a direct consequence of the crossover in the dominant relaxation mechanism, from glassy to jamming. A second major consequence is the evolution of the glassy dynamics from sub-Arrhenius to super-Arrhenius. We show that this tunable glass fragility extends to active systems analogous observations reported for passive particles. This analogy allows us to apply a dynamic scaling analysis proposed for the passive case, in order to account for our results for active systems. Finally, we discuss similarities and differences between our results and recent findings in the context of computational models of biological tissues.

active glass | reentrant dynamics | glassy dynamics | dense self-propelled particles | fragility

Significance

Dense active materials such as tissues made up of tightly packed cells have gained attention in the physics community because of the competition between slow, glass-like dynamics arising from crowding, and fluidization by active forces. We show by numerical simulations of a dense system of self-propelled particles that active forces can have nontrivial effects on the glassy behavior: As self-propulsion becomes more persistent in time, the transition from a liquid to a solid state changes from a glass transition (conventionally generated by rapid cooling) to a jamming transition (normally occurring upon athermal compression). We rationalize and organize these remarkable dynamical behaviors by constructing and analyzing the features of a critical liquid–solid surface that emerges from a dynamical scaling analysis.

The effects of active processes on glassy dynamics have fundamental importance in several biological processes, such as wound healing (1, 2), embryogenesis (3–7), asthma development (8), or cancer progression (9–15). The collective cellular dynamics during these processes exhibit a transition from a solid-like to a fluid-like state, although the static properties remain nearly the same (5, 16–20). The characteristics of the resulting glassy dynamics are broadly similar to those in equilibrium particulate systems (17–19, 21), although novel features may arise from the nonequilibrium nature of the systems. Indeed, cells are active and cellular systems are constantly evolving far from equilibrium (22, 23). Cells can also change their characteristics during various processes (24, 25), and they are extended objects for which cellular shapes closely correlate with biological functions (1, 8, 26–28). Geometric features can also differ from passive systems for the same reason; epithelial systems, for example, are always confluent, so that the cells entirely cover the space and the packing fraction may not be the most relevant parameter (5).

The complexity of active biological systems makes it challenging to gain insights into the key mechanisms driving their glassy dynamics. Simulation studies of model cellular systems have been instrumental here, showing a rigidity transition akin to the jamming transition (8, 29, 30). Furthermore, several computational studies have demonstrated that these systems exhibit nontrivial glassy behavior, such as sub-Arrhenius relaxation dynamics (31–33), possibly crossing over to super-Arrhenius behavior as the shape index (which controls cell shape) varies (32–34). It would be useful to elucidate whether these features are specific to biological tissues and vertex models, or can be observed in simpler models of active particles.

Active systems composed of self-propelled particles cannot capture all microscopic details of biological tissues but may nevertheless provide useful insights into the competition between crowding and activity. Beyond this they can also reveal what features are specific to confluent models with many-body interactions, compared to particle models with pairwise forces. In the latter models, particles self-propel under the influence of self-propulsion forces of amplitude f_0 and persistence time τ_p (18–20, 22, 23, 35–38). In fact, several biological systems can be conveniently modeled as dense systems of self-propelled particles on different lengthscales, such as for example collections of cells (16, 39), the cytoplasm (40–42), aggregates of organisms (43, 44), and synthetic active matter (45–48). Several experiments (16, 46, 49, 50) and simulation studies (51–55) have shown that active systems in their dense regime exhibit many characteristics similar to glasses (5, 18–20), such as the anomalously slow two-step

Author affiliations: [a]Tata Institute of Fundamental Research, Hyderabad 500046, India; [b]Institute for Theoretical Physics, University of Göttingen, Göttingen 37077, Germany; and [c]Gulliver, CNRS UMR 7083, Ecole Supérieure de Physique et Chimie Industrielles de la Ville de Paris, Universitéde recherche Paris Sciences et Lettres, Paris 75005, France

Author contributions: P.P., P.S., S.K.N., and L.B. designed research; P.P. performed research; P.P., P.S., S.K.N., and L.B. contributed new analytic tools; P.P., P.S., S.K.N., and L.B. analyzed data; and P.P., P.S., S.K.N., and L.B. wrote the paper.

The authors declare no competing interest.

This article is a PNAS Direct Submission.

[1]To whom correspondence may be addressed. Email: saroj@tifrh.res.in.

This article contains supporting information online at https://www.pnas.org/lookup/suppl/doi:10.1073/pnas.2516624123/-/DCSupplemental.

Published January 20, 2026.

relaxation dynamics (8) and dynamical heterogeneity (56). Recent numerical studies have also revealed nontrivial effects of activity on the glassy dynamics, such as a shifted glass transition point (51, 57, 58), changing fragility (52, 54, 59, 60), and reentrant relaxation dynamics (54, 55, 61). These active particle systems thus provide a rich yet still relatively simple framework for understanding the role of nonequilibrium fluctuations on glassy dynamics.

There are several variants of active matter models in the literature (62), sometimes categorized into dry and wet active matter. In the former, the surrounding fluid is either absent or treated implicitly within the models. In the latter, the surrounding fluid is explicitly taken into account. Since glassy effects arise in the long-time dynamics, we expect the hydrodynamic role of the surrounding fluid to be insignificant, as it affects the physics on much shorter timescales. We thus believe that the dry-wet distinction is less relevant in the present context (63, 64). Similarly, dimensionality effects are not expected to play an important role for the specific questions addressed in our study.

Theories of the equilibrium glass transition, such as the mode-coupling theory (57, 58, 65–73) and the random first-order transition approach (33, 34, 59, 74) have been extended to active glasses to rationalize numerical and experimental results. In fact, several aspects of activity-driven glassy dynamics remain equilibrium-like at a suitably defined effective temperature (52, 59). However, there are also a number of nontrivial aspects that have been reported, such as reentrant glassy dynamics (46, 55, 61), change of glass fragility (52, 54, 59, 60), and emerging velocity correlations (65). Furthermore, the specific role of τ_p on the glassy dynamics has not been elucidated fully. Crucially, how to extend and connect these results to studies of more complex biological systems remains unclear.

To address all these issues, we investigate active glassy dynamics via computer simulations of a system of soft repulsive particles. This model smoothly connects and unifies distinct physics in appropriate limits. In the limit of zero activity, the finite-temperature (T) glassy behavior is governed by a "glass point" in the limit of small but nonzero T, and a jamming transition at $T = 0$ itself. One can thus explore both jamming and glassy physics within the same system (75–79). On the other hand, the same system in the very dense limit is a good approximation of confluent cellular systems. Between these two limits the system describes the active matter physics of particulate systems, where qualitatively different regimes can be expected as the persistence time is varied. Therefore, this is a fairly rich model, which as we will demonstrate exhibits several nontrivial features that have also been reported in biological tissues. Our goal is, then, to provide a physical interpretation of the observed behaviors, in the context of a particle model that is relatively easy to study and understand. This approach will also be useful to guide and interpret future studies of biological materials and tissue models, for instance to disentangle specific effects due to the confluent nature of tissues or the possible influence of many-body forces.

Our manuscript is organized as follows. In Section 1, we introduce the model and its control parameters and explain the various limiting situations it describes. In Section 2, we present the broad glassy features for a selected set of parameters. In Section 3, we collect our results to construct the complete three-dimensional phase diagram of the model delimiting fluid and glass phases. In Section 4, we show that the location of the glass transition has a nontrivial dependence on the persistence time at fixed driving amplitude, leading to reentrant glassy dynamics. In Section 5, we show that the system displays a crossover from sub-Arrhenius to super-Arrhenius dynamics as density and persistence time are increased. In Section 6, we extend a dynamic scaling analysis proposed for equilibrium soft spheres to our soft persistent particles. In Section 7, finally, we discuss our results and provide some perspectives regarding biological tissues.

1. Model for Soft Active Particles

We consider a three-dimensional 50:50 binary mixture of particles of two types A and B, interacting via the Weeks-Chandler-Andersen purely repulsive potential. We expect that similar results will hold in two dimensions, as the effects of dimensionality on glassy dynamics are well understood (80). We assume that thermal fluctuations are not relevant and set the Brownian temperature to $T = 0$. Instead, the particles are driven by nonthermal self-propulsion forces, for which we use the AOUP (active Ornstein–Uhlenbeck particle) activity model (see *SI Appendix*, section S1 for further details). Previous studies have demonstrated that similar physics would be obtained independently of the specific model chosen for the self-propulsion or the repulsive pairwise interaction (81).

We use molecular dynamics simulations to evolve the particle position $\mathbf{r}_i$ of the ith particle using the following equation of motion:

$$\dot{\mathbf{r}}_i = \xi_0^{-1}\left[\mathbf{F}_i + \mathbf{f}_i\right], \qquad [1]$$

where ξ_0 is the friction coefficient, $\mathbf{F}_i$ is the interaction force felt by the ith particle from the other particles, and $\mathbf{f}_i$ is the active self-propulsion force. The latter follows an Ornstein–Uhlenbeck stochastic process

$$\tau_p \dot{\mathbf{f}}_i = -\mathbf{f}_i + \boldsymbol{\eta}_i, \qquad [2]$$

with $\langle \boldsymbol{\eta}_i(t)\boldsymbol{\eta}_j^{\mathrm{T}}(t')\rangle = 2f_0^2\mathbf{I}\delta_{ij}\delta(t-t')$, where "T" denotes the transpose and $\mathbf{I}$ the identity matrix. We present results using $\xi_0\sigma_{BB}^2/\epsilon$ as the time unit, with σ_{BB} the diameter of B-type particles that sets the unit length, and ϵ the energy scale of the pair potential.

The self-propulsion force $\mathbf{f}_i$ in Eq. **1** is stochastic with zero mean and correlator $\langle \mathbf{f}_i(t)\mathbf{f}_j^{\mathrm{T}}(0)\rangle = (f_0^2/\tau_p)\exp[-t/\tau_p]\mathbf{I}\delta_{ij}$. It thus has a typical amplitude $|\mathbf{f}_i| \sim f_0/\sqrt{\tau_p}$ and fluctuations that are correlated over a time of order τ_p. In the limit of very small persistence times, $\tau_p \to 0$, the propulsion forces thus become equivalent to a thermal white noise, with f_0^2 playing the role of a temperature. In the opposite limit of large persistence times, the propulsions become nearly constant random driving forces of amplitude $f_0/\sqrt{\tau_p}$.

To smoothly interpolate between these two limits, it is useful to introduce an effective temperature, T_{eff} (58, 59, 82–85), with

$$T_{\mathrm{eff}} = \frac{f_0^2}{1 + G\tau_p}, \qquad [3]$$

where G is a constant (58). This effective temperature reduces to $T_{\mathrm{eff}} \sim f_0^2$ for small persistence times and to $T_{\mathrm{eff}} \sim f_0^2/\tau_p$ for larger τ_p. The expression in Eq. **3** can be analytically justified by considering the position fluctuations of a single AOUP in a harmonic potential (86).

The concept of an effective temperature has a long history in both active and glass matter (82). For active glasses, an effective temperature naturally emerges in the long-time dynamics (57, 58, 87). It has even been shown that the relaxation dynamics for the active system agrees well with the mode-coupling scaling description using T_{eff}. Using this effective temperature description for the relaxation dynamics and

comparing it with the mode-coupling theory scaling relations (*SI Appendix*, Fig. S5), we estimate $G \simeq 0.5$ for the current system. For the present purposes, T_{eff} is a useful quantity as it reduces to a genuine thermodynamic temperature in the small τ_p limit, but our results do not rely on any thermodynamic interpretation far from equilibrium.

The three control parameters of the model are the persistence time τ_p, the amplitude f_0 in the noise term in Eq. **2** and the volume fraction ϕ. We will systematically vary them to fully characterize the part of the phase diagram where the system becomes glassy. It is first interesting to consider the various physical limits captured by this model.

Small persistence time, $\tau_p \to 0$. The phase diagram becomes effectively two-dimensional in the equilibrium limit $\tau_p \to 0$, where the system becomes equivalent to a Brownian system with the two control parameters temperature and density, ($T_{\text{eff}} \sim f_0^2$, ϕ), as usual in equilibrium fluids. The smooth approach to the Brownian limit makes the AOUP model in Eqs. **1** and **2** appealing. In this limit, the physics becomes strictly equivalent to the one of soft repulsive spheres at thermal equilibrium, as studied extensively in ref. 76.

Small force amplitude, $f_0 \to 0$. For finite τ_p, another interesting limit is the one where $f_0 \to 0$. In this limit, the amplitude of the self-propulsion force $\mathbf{f}_i$ in Eq. **1** becomes much smaller than that of the interaction forces $\mathbf{F}_i$, so that particles will no longer interpenetrate (unless forced to do so by a high volume fraction ϕ). As a consequence, the system behaves as self-propelled hard spheres with a finite persistence time τ_p. The phase diagram is again two-dimensional, with (τ_p, ϕ) as control parameters. Such self-propelled hard spheres have been studied in several past works (51, 88) and undergo a nonequilibrium glass transition, at a volume fraction $\phi_d(\tau_p)$ that depends continuously on the persistence time. These special "glass points" in the phase diagram will play a prominent role in our dynamic scaling analysis in Section 6.

Large persistence time, $\tau_p \to \infty$. The final interesting limit is that of infinitely persistent particles obtained when $\tau_p \to \infty$. In that limit, particles are driven by frozen random forces whose amplitudes $|f_i| \sim f_0/\sqrt{\tau_p}$ become vanishingly small compared to interparticle forces, in the absence of any other source of fluctuations. By construction, the system undergoes in this limit a jamming transition at a packing fraction ϕ_J, between a flowing fluid and a solid phase. We expect the dynamics in this "jamming" limit to differ qualitatively from the glassy dynamics observed near glass transitions (89).

2. Characterizing the Glassy Dynamics

We characterize the glassy dynamics via the self-intermediate scattering function, $F_s(k, t)$, at wavevector k and time t, defined as

$$F_s(k,t) = \frac{1}{N}\left\langle \sum_{i=1}^{N} e^{i\mathbf{k}\cdot(\mathbf{r}_i(t+t_0)-\mathbf{r}_i(t_0))} \right\rangle, \qquad [4]$$

and by the mean-squared displacement

$$\text{MSD}(t) = \left\langle \frac{1}{N}\sum_{i=1}^{N} [\mathbf{r}_i(t+t_0) - \mathbf{r}_i(t_0)]^2 \right\rangle, \qquad [5]$$

where N is the total number of particles, $\mathbf{r}_i(t)$ is the position of the ith particle at time t, and $\langle \ldots \rangle$ denotes an average over independent configurations and over the time origins t_0 taken at steady state. For convenience, we choose k as the position of the first peak of the static structure factor of the passive system at $\phi = 0.65$; this first peak position does not change significantly at other values of ϕ (*SI Appendix*, Fig. S1). We first ask how the dynamics varies with f_0 at constant τ_p, and then explore the evolution with τ_p.

We show the time dependence of $F_s(k, t)$ and MSD(t) at constant $\phi = 0.65$ and $\tau_p = 10^{-2}$ with varying f_0^2 in Fig. 1 *A* and *B*. The self-intermediate scattering function $F_s(k, t)$ first decays toward a nonzero plateau value and at later times to zero; see Fig. 1*A*. The plateau region of $F_s(k, t)$ corresponds to subdiffusive motion in the MSD, which only becomes diffusive at much longer times; see Fig. 1*B*. As f_0 increases, the decay of $F_s(k, t)$ and the transition in the MSD from subdiffusive to diffusive behavior occur at shorter times. Overall the dynamical characteristics of $F_s(k, t)$ and MSD with increasing f_0 are similar to those of equilibrium supercooled fluids with increasing temperature T. For further quantification one can define the relaxation time τ_α as the value of t for which $F_s(k, t)$ decays to $1/e$, explicitly $F_s(k, \tau_\alpha) = 1/e$. From Fig. 1*A*, it is then clear that τ_α decreases as f_0 increases. We have explored the dynamics at several other packing fractions ϕ, and the qualitative behavior remains the same.

We now characterize the liquid-glass phase boundary at constant τ_p. For this purpose, we first obtain τ_α for several values of ϕ at constant f_0. Fig. 1*C* shows the state points we have explored and the corresponding values of τ_α. We then use a logarithmic fit,

$$\ln \tau_\alpha = A + B/(\phi_c - \phi), \qquad [6]$$

using A, B, and ϕ_c as fit parameters, to obtain the liquid-glass critical point $\phi_c(f_0^2, \tau_p)$ for fixed f_0 and τ_p. The expression [**6**] is formally analogous to the Vogel–Fulcher–Tammann (VFT) relation describing the relaxation time of molecular liquids, and implies that the system becomes a glass at the point where τ_α diverges, i.e. for $\phi = \phi_c(f_0^2, \tau_p)$. We repeat the above fitting procedure for a range of f_0 and use the results to construct the liquid-glass critical line in the (f_0, ϕ) plane at fixed τ_p, as shown in Fig. 1*C* for the specific value $\tau_p = 10^{-2}$. For this small τ_p, the critical glass line in the (f_0, ϕ) plane is by construction very close to the equilibrium glass line obtained for $\tau_p \to 0$, with f_0^2 playing the role of temperature (75, 76).

The results in this section are broadly consistent with existing literature on active glassy systems, where the effects of activity remain equilibrium-like at a suitably defined effective temperature as long as τ_p is small (52, 54, 58, 59). In the next sections, we explore a much broader range of control parameters, which will allow us to reveal additional effects that are nontrivial.

3. Three-Dimensional Phase Diagram

We now construct the three-dimensional liquid-glass phase diagram in the full control parameter space (f_0, τ_p, ϕ) to understand how the persistence time τ_p changes the results set out in Section 2 above. For this purpose, we obtain the critical lines $\phi_c(f_0^2, \tau_p)$ by repeating the fitting procedure shown in Fig. 1*C* for several values of τ_p. This numerical exploration of the three-dimensional space represents a significant computational effort, given that it requires simulations scanning a range of volume fractions ϕ for each pair of values (f_0, τ_p). This large computational effort is useful, as it allows us to recover within a single approach several results obtained independently in various limits, which we

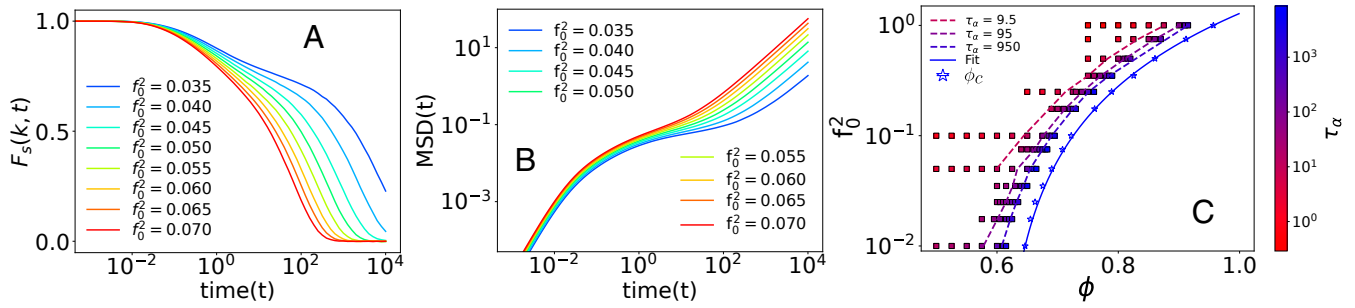

Fig. 1. Characterization of the active glassy dynamics. (*A*) The two-step decay of $F_S(k,t)$ becomes faster with increasing f_0 at constant $\phi = 0.65$ and $\tau_P = 10^{-2}$. (*B*) The corresponding MSD has a subdiffusive to diffusive crossover at intermediate times, and particle motion becomes faster with increasing f_0. (*C*) The liquid-glass (f_0, ϕ) phase diagram for $\tau_P = 10^{-2}$. Squares represent the simulated state points with the corresponding τ_α color-coded and dashed lines representing iso-τ_α contours. Stars are the ϕ_C values obtained using Eq. **6**, while the solid line connecting them is a fit to Eq. **8**.

can rationalize and organize in the scaling approach developed below. The symbols in Fig. 2*A* show the resulting critical lines, $\phi_c(f_0^2, \tau_p)$ in the (f_0, ϕ) plane for several values of τ_p. Similar data were obtained in ref. 55 using the diffusivity, but the detailed characteristics and consequences were not fully explored.

Several features are immediately apparent from the data in Fig. 2*A*. First, $\phi_c(f_0^2, \tau_p)$ displays a nontrivial evolution with τ_p. As τ_p increases, the critical lines become more vertical, which implies that the glass transition line becomes less sensitive to f_0^2 for larger persistence times. Also, the $\phi_c(f_0^2 \to 0, \tau_p)$ values shift to higher packing fractions and appear to saturate at very large τ_p. Finally, the evolution of ϕ_c with τ_p exhibits opposite trends for small and large values of f_0, respectively. We will relate these observations below to the physical behavior of the system.

To proceed, we first propose an analytical description of the critical surface delimiting fluid and glass phases. It is convenient to first introduce the notation

$$\phi_d(\tau_p) \equiv \phi_c(f_0^2 \to 0, \tau_p), \qquad [7]$$

which defines the location of the glass transition in the self-propelled hard sphere limit. We then fit the critical lines in Fig. 2*A* with a power law

$$f_0^2 = a[\phi_c(f_0^2, \tau_p) - \phi_d]^{2/\beta}, \qquad [8]$$

where the prefactor a, the exponent β and the critical density ϕ_d are used as fit parameters for each τ_p value. The resulting fitted functions are displayed as lines in Fig. 2*A*. The fits confirm that $\phi_d(\tau_p)$ first increases with τ_p and then saturates at larger τ_p (*SI Appendix*, Fig. S4). The prefactor $a(\tau_p)$ monotonically increases with increasing τ_p (*SI Appendix*, Fig. S3). On the other hand, the exponent $\beta(\tau_p)$ has a weak nonmonotonic τ_p-dependence (*SI Appendix*, Fig. S3). In the SM, we propose empirical fitting forms to represent the τ_p-dependence of these three constants, which work well (*SI Appendix*, section S4).

We are finally in a position to collect the above fits of our simulation data into a liquid-glass surface in the three-dimensional phase diagram shown in Fig. 2*B*, using as axes (f_0^2, ϕ, τ_p). The glass phase is located in the large-ϕ, low-f_0 corner of this parameter space, with nontrivial evolution with τ_p and opposite trends at large and small τ_p values. In the next two sections, we explore two major consequences of the shape of this phase diagram.

4. Reentrant Relaxation Dynamics

We first establish the presence of reentrant glassy dynamics, where τ_α has a nonmonotonic variation with changing τ_p, as a consequence of the τ_p dependence of the critical surface constructed in Fig. 2*B*. We present in Fig. 3*A* the evolution of τ_α as a function of the persistence time τ_p for a range of values of f_0^2. These data indeed show that τ_α has a nontrivial nonmonotonic

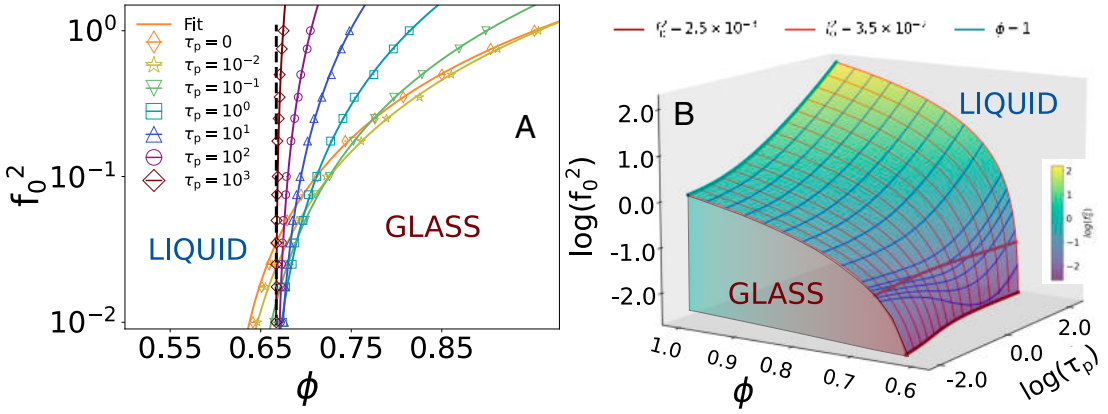

Fig. 2. Constructing the three-dimensional phase diagram. (*A*) The liquid-glass critical lines (symbols) determined via Eq. **6** for different values of τ_p. These lines are themselves fitted to a power law form, Eq. **8**, shown as lines. The vertical dashed line indicates the limit $\phi_d(\tau_p \to \infty)$. (*B*) The three-dimensional liquid-glass phase diagram can then be reconstructed from the fitted analytical expressions, with the glass phase occurring for large ϕ and low f_0, with a nontrivial evolution with τ_p. Two iso-f_0^2 lines are shown; the one corresponding to $f_0^2 = 3.5 \times 10^{-2}$ is nonmonotonic.

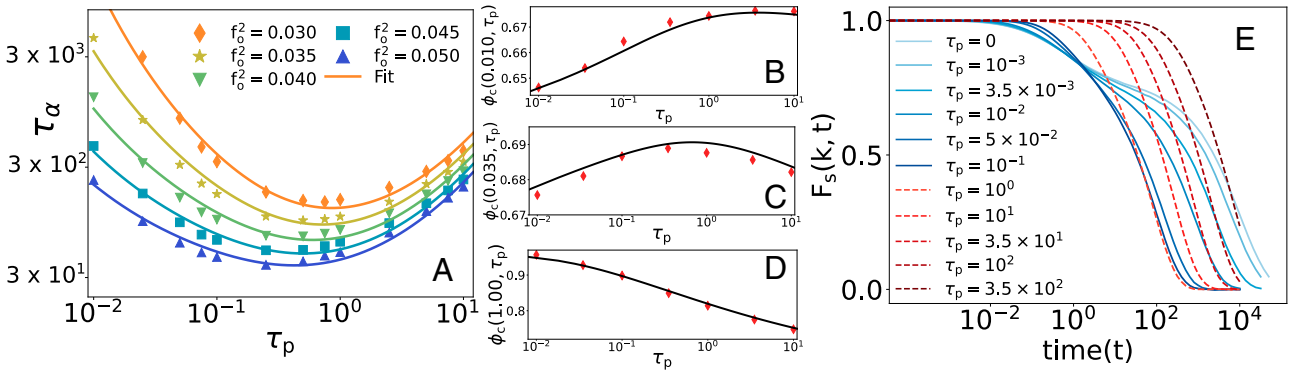

Fig. 3. Reentrant glassy dynamics. (*A*) Nonmonotonic behavior of τ_α as a function of τ_p at various f_0^2 and $\phi = 0.65$. The lines combine Eqs. **6** and **8** (*SI Appendix*, Table S1). (*B–D*) The dependence of $\phi_c(f_0^2, \tau_p)$ on τ_p for a small, an intermediate and a large value of f_0^2, showing a change from a monotonically increasing to a monotonically decreasing trend, with nonmonotonic variation for the intermediate f_0^2. Lines represent the analytical description in Eq. **9**. (*E*) Time decay of $F_s(k, t)$ for $\phi = 0.65$ and $f_0^2 = 0.045$ and various τ_p. The intermediate time plateau at small τ_p, i.e. in the glassy regime, disappears at large τ_p in the jamming regime.

evolution with the persistence time τ_p at fixed values of ϕ and f_0^2.

Qualitatively this behavior arises because of the opposite trends mentioned above: The critical liquid-glass density increases with τ_p at small f_0, whereas it decreases at large f_0. These contrasting trends create an intermediate range of f_0 where the critical density is nonmonotonic in τ_p. We show this explicitly in Fig. 3 *B–D* where we follow the evolution with τ_p of $\phi_c(f_0^2, \tau_p)$ for a small, intermediate and large value of f_0 and observe increasing, nonmonotonic, and decreasing variation with τ_p, respectively.

To describe this reentrant behavior more quantitatively, we start from Eq. **8** and rewrite the equation describing the critical glass surface $\phi_c(f_0^2, \tau_p)$ as

$$\phi_c(f_0^2, \tau_p) = [f_0^2/a]^{\beta/2} + \phi_d(\tau_p). \qquad [9]$$

This critical density is, by construction, controlled by the second term when $f_0 \to 0$, so that ϕ_c increases with τ_p along with ϕ_d. For large f_0, on the other hand, the first term dominates and ϕ_c then decreases with τ_p due to the increase of a (recall *SI Appendix*, Fig. S3). The lines in Fig. 3 *B–D* confirm that the empirical description of the glass surface obtained in Section 3 describes the numerical data, and thus the reentrant dynamics, very well.

To conclusively establish that the shape of the critical surface does describe the reentrant behavior, we use Eq. **6**. This expression can be obtained within the random-first-order transition theory, which constitutes a microscopic theory of the glass transition (90, 91) that has been extended for active systems (59, 74). Using $\phi_c(f_0^2, \tau_p)$ in Eq. **6**, we obtain τ_α as

$$\ln \tau_\alpha = A + \frac{B}{c[f_0^2/a(\tau_p)]^{\beta(\tau_p)/2} + \phi_d(\tau_p) - \phi}, \qquad [10]$$

where we have included the fitting parameter c to account for the activity-dependence of A and B (the value of c is nearly 1; see *SI Appendix*, section S8 for further details). The lines in Fig. 3*A* are the plots of Eq. **10** with the values of c as given in *SI Appendix*, Table S1. The excellent agreement between the simulation results and Eq. **10** demonstrates that it is indeed the critical surface shape that governs the reentrant behavior. Indeed, neglecting the fit factor c (*SI Appendix*, section S8), the key first two terms in the denominator of Eq. **10** just correspond to ϕ_c. The competition between these terms determines, for given f_0^2 and ϕ, the location $\tau_{p,\min}$ of the reentrant minimum in τ_α (Fig. 3*A*). To understand qualitatively how $\tau_{p,\min}$ varies with f_0, notice from Fig. 3*B* that, for small f_0, ϕ_c is increasing with τ_p and hence τ_α is decreasing, corresponding to $\tau_{p,\min} \to \infty$. For large f_0 the situation is reversed (Fig. 3*D*) and $\tau_{p,\min} \to 0$. In the intermediate range of f_0, where $\tau_{p,\min}$ is finite, it must therefore decrease with increasing f_0 consistent with the trend visible in Fig. 3*A*.

The reentrant dynamics observed when τ_p increases is accompanied by a qualitative change in the physical relaxation process, since the system crosses over from near-equilibrium glassy relaxation dynamics when $\tau_p \to 0$ to nonthermal jamming physics when $\tau_p \to \infty$, as explained in Section 1. This evolution from glass to jamming physics is captured by the behavior of the self-intermediate scattering function shown in Fig. 3*E*, which we show here for constant $\phi = 0.65$ and $f_0^2 = 0.045$ while varying τ_p over a broad range of five orders of magnitude. At small τ_p, $F_s(k, t)$ shows the characteristic two-step relaxation decay typical of glassy relaxation. However, at very large τ_p, $F_s(k, t)$ decays in a single step with no intermediate plateau, as usually observed in driven systems in the absence of thermal fluctuations (89, 92). As expected, the MSD also shows a similar change of behavior with changing τ_p (*SI Appendix*, Fig. S6). Beyond these qualitative changes, the nonmonotonic dependence on τ_p of the final decay time of $F_s(k, t)$ is also evident from Fig. 3*E*.

Reentrant behavior appears in a variety of systems, including colloidal suspensions of sticky hard spheres (93) and fluids confined within periodic potentials (94, 95). In these equilibrium colloidal systems, reentrance is typically governed by large changes in the static structure. By contrast, reentrant behavior in active systems has been described via changes in the caging dynamics (61, 63, 68) or via effective attractive interactions (46, 55). Our work provides a complementary perspective on the mechanism underlying reentrant behavior in active systems.

5. Tunable Fragility and Sub-Arrhenius to Super-Arrhenius Crossover

Several past studies have shown that activity may change the glass fragility of self-propelled systems (52, 54, 59). A tunable fragility was also reported in the context of vertex and Voronoi models

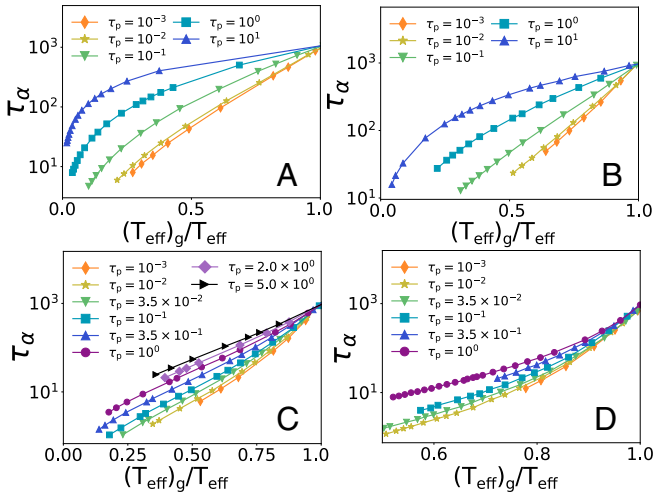

Fig. 4. Evolution of the glass fragility shown using Angell plots. Each panel represents data obtained at a given packing fraction, ϕ with (*A*) $\phi = 0.625$, (*B*) $\phi = 0.650$, (*C*) $\phi = 0.693$, and (*D*) $\phi = 0.800$, and each panel contains data for a range of τ_p values. The glass fragility decreases systematically with increasing τ_p, and increases systematically with increasing ϕ. The behavior of τ_α crosses over from sub-Arrhenius at low ϕ and/or large τ_p to super-Arrhenius for large ϕ and/or small τ_p.

of biological tissues (31–34, 96). Here, we show that the glass fragility in our model depends on both τ_p and packing fraction ϕ, with the physics being again controlled by the evolution of the glass critical surface constructed in Section3.

In thermal equilibrium, the glass fragility characterizing slow dynamics is usually determined by following the temperature evolution of the structural relaxation time, $\tau_\alpha(T)$. Systems that exhibit a simple Arrhenius behavior are strong, whereas a more pronounced temperature dependence (also called super-Arrhenius) corresponds to fragile glasses. Fragility is graphically captured in Angell plots, where the logarithm of τ_α is shown as a function of the inverse temperature so that data points for a strong glass lie on a straight line.

To investigate fragility in active systems, we generalize this equilibrium analysis and follow the evolution of the structural relaxation time τ_α as a function of the effective temperature $T_{\text{eff}} = f_0^2/(1 + G\tau_p)$ defined in Eq. **3**. We tune T_{eff} by varying f_0^2, at fixed values of ϕ and τ_p. We construct the active analogue of Angell plots showing the logarithm of τ_α as a function of inverse T_{eff}. We refine this representation by going to a rescaled version of the Angell plot, scaling T_{eff} by its value $(T_{\text{eff}})_g$ at the computer glass transition defined as $\tau_\alpha[(T_{\text{eff}})_g] = 10^3$. This scaling allows for a simpler visualization of the evolution of the glass fragility with control parameters.

We collect the results of this analysis in the four panels of Fig. 4. Each panel represents an Angell plot constructed for a given packing fraction from $\phi = 0.625$ to $\phi = 0.800$, and the various curves in each panel are obtained for different values of the persistence time.

These data reveal several intriguing features. In each panel, we observe that glass fragility decreases when τ_p increases at a fixed density, a trend which holds at all densities. At the lowest density (Fig. 4*A*), we observe that all systems display sub-Arrhenius relaxation, that is, the relaxation time grows more slowly than in an Arrhenius fashion. This is not observed at large density (Fig. 4*D*), where all systems now exhibit super-Arrhenius relaxation, very much like conventional passive molecular glass-forming materials. Therefore, the glass fragility increases both when τ_p decreases and when ϕ increases, with a peculiar sub-Arrhenius regime found at low enough ϕ and large enough τ_p.

A qualitatively similar evolution with the density of the glass fragility was observed previously in the Brownian limit, $\tau_p \to 0$, for a similar model of soft repulsive spheres (75, 76). The microscopic explanation is relatively straightforward. When decreasing T at constant ϕ, the system ends up in an equilibrium hard sphere fluid if $\phi < \phi_d$. As a result, $\tau_\alpha(T \to 0)$ does not diverge, and this qualitatively explains the apparent sub-Arrhenius behavior. Instead, above the critical density ϕ_d, the system crosses a glass transition at a finite T, and as a consequence, the relaxation dynamics appears to diverge at a finite T, which gives rise to a super-Arrhenius temperature dependence. In this view, the glass fragility is changing continuously with density, and it is primarily controlled by the distance to the critical density ϕ_d that characterizes the $T \to 0$ hard sphere limit. Note that in this physical explanation of the evolution of fragility, the softness of the particles plays no role. In Brownian colloidal systems, particle softness has likewise been shown to play only a limited role in directly controlling glass fragility (97). In some soft charged colloids, osmotic deswelling has been shown to produce a large fragility change (98, 99), but this is unrelated to our observations.

The above qualitative interpretation easily extends to our observation in active systems, which we rationalize using the three-dimensional phase diagram in Fig. 4*B*. When decreasing T_{eff} (and thus f_0^2) at constant τ_p the system either ends in a fluid at ϕ below ϕ_d, or in a glass at ϕ above ϕ_d. This explanation is valid for any value of the persistence time, and it directly explains the ϕ dependence of the glass fragility reported in Fig. 4. In addition, since ϕ_d increases with τ_p, the glass fragility observed at a given ϕ must decrease with τ_p because it is mostly controlled by the distance to ϕ_d.

6. Dynamic Scaling Near the Hard Sphere Non-Equilibrium Glass Transition

For the equilibrium glassy dynamics of soft repulsive spheres (75, 76), a dynamic scaling approach has previously been proposed to rationalize the qualitative variation across the (ϕ, T) plane. This analysis disentangles two aspects in the growth of τ_α. First, τ_α grows at low T simply because the thermal velocity of the system decreases, thus slowing down the relevant microscopic timescale τ_{mic} controlling particle motion. For thermal systems, $\tau_{\text{mic}} \propto 1/\sqrt{T}$, and it is thus convenient to rescale τ_α by τ_{mic} to single out the effect of glassiness.

The second, more interesting, cause for slow dynamics is the emergence of complex and cooperative glassy dynamics. For this part, the dynamic scaling amounts to first identifying the physical behavior in the hard sphere limit ($T \to 0$), and to then assuming that thermalized soft spheres essentially obey the same physics as hard spheres, but at an "effective" value $\phi_{\text{eff}} < \phi$ of the packing fraction, so that thermal soft spheres essentially appear as "small" hard spheres. Mathematically, the first assumption is a statement about the hard sphere $T \to 0$ limit, written as

$$\tau_\alpha \sim \exp[A/(\phi_0 - \phi)^\delta], \qquad [11]$$

which becomes equivalent to Eq. **6** when $\delta = 1$. The connection between soft and hard particles then suggests the following scaling form:

$$\tau_\alpha \sim \exp\left[\frac{A}{|\phi_0 - \phi|^\delta} F_\pm\left(\frac{|\phi_0 - \phi|^\mu}{T}\right)\right], \qquad [12]$$

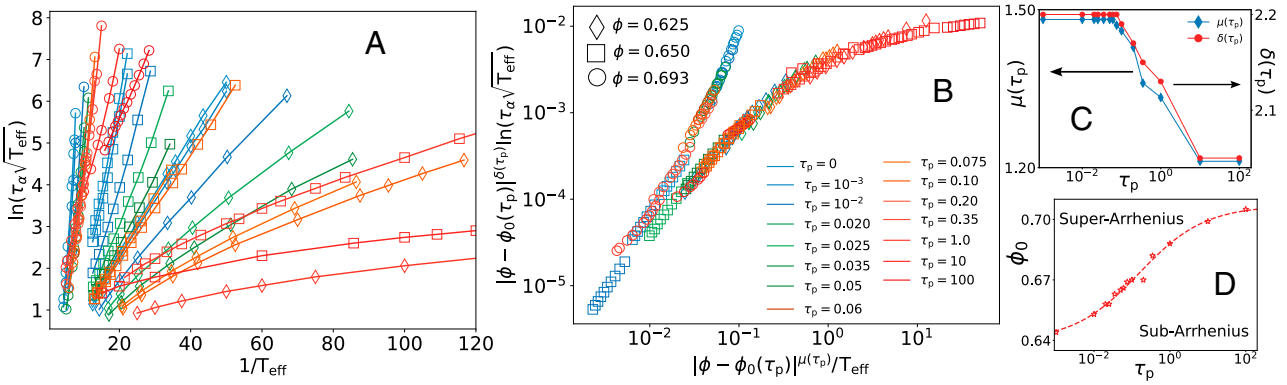

Fig. 5. Dynamic scaling analysis collapses the glassy dynamics of active particles. (*A*) Angell plot using the rescaled relaxation time $\tau_\alpha\sqrt{T_{\rm eff}}$ as a function of $1/T_{\rm eff}$. Different symbols are for different ϕ, different colors are for different τ_p. (*B*) Global data collapse along the two branches describing the $\phi < \phi_0$ sub-Arrhenius and $\phi > \phi_0$ super-Arrhenius family of curves, as described in Eq. **12**. (*C*) The exponents δ and μ depart weakly from their equilibrium value as τ_p increases. (*D*) The critical hard sphere density $\phi_0(\tau_p)$ changes smoothly with τ_p.

where two scaling functions $F_\pm(x)$ are introduced to describe the respective behavior for densities above ϕ_0, for $F_+(x)$, and below for $F_-(x)$. The hard sphere behavior in Eq. **11** for $T \to 0$ imposes $F_-(x \to \infty) = 1$ and $F_+(x \to \infty) = +\infty$. Similarly, the continuity of the data for $\phi = \phi_0$ imposes that $F_-(x) \sim F_+(x) \sim x^{\delta/\mu}$ for $x \to 0$, so that $\tau_\alpha \sim \exp(A/T^{\delta/\mu})$ exactly at $\phi = \phi_0$.

The steps needed to extend the dynamic scaling analysis performed in equilibrium to active systems are relatively straightforward. The first step is to replace T with the effective temperature $T_{\rm eff}$ in Eq. **3**. In a second step, we rescale the relaxation time τ_α with a microscopic timescale $\tau_{\rm mic} \sim 1/\sqrt{T_{\rm eff}}$. In a third step we generalize Eq. **12** by allowing the exponents δ and μ, and the critical packing fraction ϕ_0, to depend on the persistence time τ_p. The scaling functions $F_\pm(x)$ could in principle also depend on τ_p, but we find that this is not necessary to achieve a good collapse of the data.

We now show how to apply this scaling procedure to our data. In Fig. 5*A*, we plot how the rescaled relaxation times $\tau_\alpha/\tau_{\rm mic} \sim \tau_\alpha\sqrt{T_{\rm eff}}$ depend on the effective temperature $T_{\rm eff}$ for multiple combinations of values of τ_p and ϕ. In this rescaled form, the data at $\phi < \phi_0$ visibly saturate to a finite relaxation time in the $T_{\rm eff} \to 0$ hard sphere limit, which leads to sub-Arrhenius temperature evolution. By contrast, the data for $\phi > \phi_0$ do not show any saturation and their evolution is compatible with a divergence at a finite effective temperature, which leads to super-Arrhenius temperature evolution.

We are now in a position to apply Eq. **12** to our data. In practice, we find that the largest value of the packing fraction, $\phi = 0.8$, is too far above the critical density ϕ_0 and does not provide a good data collapse. Therefore, we did not use these data for the scaling analysis. The data collapse procedure is somewhat tedious as it requires the simultaneous identification of the free parameters δ, μ and ϕ_0 for each τ_p. In practice, we initialized the fitting process with the values obtained in equilibrium (76) and slowly varied the fit parameters to achieve a satisfactory result for all τ_p values. The outcome of this analysis is shown in Fig. 5*B*, showing the data collapse of the relaxation data along the two branches described by F_- and F_+, while the fitted parameters are shown in Fig. 5 *C* and *D*. The exponents δ and μ vary weakly with τ_p and show only small departures from their equilibrium values (corresponding to $\tau_p \to 0$). The critical density ϕ_0 increases gradually with τ_p and saturates at large persistence times. As expected, it closely mirrors the evolution of ϕ_d discussed above (*SI Appendix*, Fig. S4), as they both describe the same hard sphere dynamics using slightly different functional forms, Eqs. **6** and **11**.

The quality of the data collapse in Fig. 5*B* with weak variations of (δ, μ) and scaling functions $F_-(x)$ and $F_+(x)$ that are independent of τ_p demonstrates that the scaling analysis proposed for equilibrium soft particles also applies to self-propelled soft particles. Only one physical quantity varies significantly with τ_p in this analysis, the critical density $\phi_0(\tau_p)$ that describes the $T_{\rm eff} \to 0$ limit of self-propelled hard spheres. This promotes the "glass point" ϕ_0 of ref. 76 to a continuous "glass line" $\phi_0(\tau_p)$ with a dependence on the persistence time. A physical outcome of the data collapse in Fig. 5 is the demonstration that glass fragility of active particles is directly controlled by the distance to the critical density $\phi_0(\tau_p)$, while the functional forms of the two scaling functions account for the crossover from sub-Arrhenius to super-Arrhenius.

7. Discussion and Perspectives

We have studied the glassy dynamics in an active system of self-propelled soft spherical particles. This model system contains as limit cases thermal soft spheres and persistent self-propelled hard spheres, while for large f_0 and τ_p it describes self-propelled soft particles and so connects qualitatively also to the physics of confluent biological tissues. This broad range of physical behaviors captured by the model leads to a rich phenomenology, which we reveal here by performing a full exploration of the three-dimensional phase diagram (f_0, τ_p, ϕ).

The construction and quantitative analysis of the three-dimensional phase diagram and its various limits allowed us to account for two nontrivial dynamic features: reentrant glassy dynamics that emerges when τ_p is varied at fixed ϕ and f_0 and a glass fragility that is tuned by both changing τ_p and ϕ. Our analysis generalizes, and provides a simple interpretation for, related previous reports of anomalous dynamics in self-propelled particle systems (46, 55, 61). Our central conclusion is that the effect of activity is very well captured by the known equilibrium scaling description (76), provided one promotes the hard sphere glass point ϕ_0 to a hard sphere glass line $\phi_0(\tau_p)$ that depends continuously on the persistence time.

Interestingly, along this glass line of the active system one is effectively moving smoothly from a glass transition for small persistence times τ_p to a jamming transition for large τ_p (35–38) as shown by the disappearance of the intermediate plateau in

the relaxation functions with increasing τ_p. Microscopically, this behavior can be rationalized by analogy with the physics of passive glasses subjected to mechanical deformation by steady shear (89, 92): Here one, also finds a smooth change between two distinct regimes, controlled by temperature. When thermal fluctuations are significant, corresponding to our active glasses at small τ_p, relaxation under sufficiently slow shear proceeds by thermal activation across energy barriers. For times shorter than the barrier crossing time, particles can only relax partially by "rattling" in cages formed by their neighbors, causing plateaus in typical relaxation functions. In the athermal regime, on the other hand, relaxation is driven by barriers disappearing via saddle-node bifurcations as the energy landscape is gradually deformed by the applied shear. For our active systems, this is analogous to the slow tilting of the energy landscape by active forces (36, 100, 101) in the large τ_p regime; either way, the relaxation has no analog of particles rattling in cages at early times, and relaxation functions therefore do not show plateaus.

An interesting perspective for future research is to connect the behavior of soft active particles we have studied here to the physics revealed by studies of model systems for confluent epithelial tissues. In these models, the packing fraction ϕ does not control the physics as in soft particles as it is effectively fixed to unity. Instead there is a structural parameter governing the behavior of the system, the so-called target perimeter p_0 (5, 18, 30, 33). This drives the system from fluid-like states at large p_0 to solid-like behavior at low p_0, in a manner analogous to $1/\phi$ in particle systems. In spite of these important differences, the parameters p_0 and ϕ play similar roles insofar as they control the transition from fluid to solid response, in the absence of thermal fluctuations and active forces. Intriguingly, there are several reports of sub-Arrhenius to super-Arrhenius crossover in the literature as p_0 is varied (31–34), suggesting a possible analogy with soft particles. Reentrant dynamics also exists in variants of these model systems (102). Future work should explore whether the analogy can be made more quantitative, and whether the analysis carried out here can also be useful to rationalize the characteristics of the glassy dynamics of biological tissues and its interplay with jamming physics, thus hopefully illuminating the role of many-body forces and confluence in the physics of tissue models.

Data, Materials, and Software Availability. All study data are included in the article and/or *SI Appendix*.

ACKNOWLEDGMENTS. P.P. and S.K.N. acknowledge the support of the Department of Atomic Energy, Government of India, under Project identification No. RTI 4007. L.B. acknowledges the support of the French Agence Nationale de la Recherche (ANR), under grants ANR-20-CE30-0031 (project THEMA) and ANR-24-CE30-0442 (project GLASSGO). P.S. acknowledges funding by the Deutsche Forschungsgemeinschaft (DFG, German Research Foundation) under Project-ID 449750155, RTG 2756, Project A5. P.S. and S.K.N. thank the Erwin Schrödinger International Institute for Mathematics and Physics (ESI), University of Vienna (Austria) for the invitation to participate in the Thematic Program "Linking Microscopic Processes to the Macroscopic Rheological Properties in Inert and Living Soft Materials" in 2024 where part of this work has been carried out.

1. M. Poujade *et al.*, Collective migration of an epithelial monolayer in response to a model wound. *Proc. Natl. Acad. Sci. U.S.A.* **104**, 15988–15993 (2007).
2. M. Vishwakarma, B. Thurakkal, J. P. Spatz, T. Das, Dynamic heterogeneity influences the leader-follower dynamics during epithelial wound closure. *Philos. Trans. R. Soc. B Biol. Sci.* **375**, 20190391 (2020).
3. A. Mongera *et al.*, A fluid-to-solid jamming transition underlies vertebrate body axis elongation. *Nature* **561**, 401 (2018).
4. J. A. Park, L. Atia, J. A. Mitchel, J. J. Fredberg, J. P. Butler, Collective migration and cell jamming in asthma, cancer and development. *J. Cell Sci.* **129**, 3375–3383 (2016).
5. L. Atia, J. J. Fredberg, N. S. Gov, A. F. Pegoraro, Are cell jamming and unjamming essential in tissue development? *Cells and Dev.* **168**, 203727 (2021).
6. D. T. Tambe *et al.*, Collective cell guidance by cooperative intercellular forces. *Nat. Mat.* **10**, 469 (2011).
7. E. M. Schötz, M. Lanio, J. A. Talbot, M. L. Manning, Glassy dynamics in three-dimensional embryonic tissues. *J. R. Soc. Interface* **10**, 20130726 (2013).
8. J. A. Park *et al.*, Unjamming and cell shape in the asthmatic airway epithelium. *Nat. Mat.* **14**, 1040–1048 (2015).
9. P. Friedl, K. Wolf, Tumour-cell invasion and migration: Diversity and escape mechanisms. *Nat. Rev. Cancer* **3**, 362–374 (2003).
10. P. Friedl, D. Gilmour, Collective cell migration in morphogenesis, regeneration and cancer. *Nat. Rev. Mol. Cell Biol.* **10**, 445 (2009).
11. A. N. Malmi-Kakkada, X. Li, H. S. Samanta, S. Sinha, D. Thirumalai, Cell growth rate dictates the onset of glass to fluidlike transition and long time superdiffusion in an evolving cell colony. *Phys. Rev. X* **8**, 021025 (2018).
12. S. Sinha, A. N. Malmi-Kakkada, X. Li, H. S. Samanta, D. Thirumalai, Spatially heterogeneous dynamics of cells in a growing tumor spheroid: Comparison between theory and experiments. *Soft Matter* **16**, 5294–5304 (2020).
13. A. Palamidessi *et al.*, Unjamming overcomes kinetic and proliferation arrest in terminally differentiated cells and promotes collective motility of carcinoma. *Nat. Mat.* **18**, 1252–1263 (2019).
14. K. J. Streitberger *et al.*, How tissue fluidity influences brain tumor progression. *Proc. Natl. Acad. Sci. U.S.A.* **117**, 128 (2020).
15. J. A. Mitchel *et al.*, In primary airway epithelial cells, the unjamming transition is distinct from the epithelial-to-mesenchymal transition. *Nat. Commun.* **11**, 5053 (2020).
16. T. E. Angelini *et al.*, Glass-like dynamics of collective cell migration. *Proc. Natl. Acad. Sci. U.S.A.* **108**, 4714–4719 (2011).
17. L. Berthier, G. Biroli, Theoretical perspective on the glass transition and amorphous materials. *Rev. Mod. Phys.* **83**, 587–645 (2011).
18. S. Sadhukhan, S. Dey, S. Karmakar, S. K. Nandi, A perspective on active glassy dynamics in biological systems. *Eur. Phys. J. Spec. Top.* **233**, 3193 (2024).
19. L. Berthier, E. Flenner, G. Szamel, Glassy dynamics in dense systems of active particles. *J. Chem. Phys.* **150**, 200901 (2019).
20. L. M. C. Janssen, Active glasses. *J. Phys. Condens. Matter* **31**, 503002 (2019).
21. R. Higler, J. Krausser, J. van der Gucht, A. Zaccone, J. Sprakel, Linking slow dynamics and microscopic connectivity in dense suspensions of charged colloids. *Soft Matter* **14**, 780 (2018).
22. S. Ramaswamy, The mechanics and statistics of active matter. *Annu. Rev. Condens. Matter Phys.* **1**, 323 (2010).
23. M. C. Marchetti *et al.*, Hydrodynamics of soft active matter. *Rev. Mod. Phys.* **85**, 1143 (2013).
24. J. P. Thiery, Epithelial-mesenchymal transitions in tumour progression. *Nat. Rev. Cancer* **2**, 442 (2002).
25. J. P. Thiery, H. Acloque, R. Y. Huang, M. A. Nieto, Epithelial-mesenchymal transitions in development and disease. *Cell* **139**, 871 (2009).
26. H. Z. Sailem, C. Bakal, Identification of clinically predictive metagenes that encode components of a network coupling cell shape to transcription by image-omics. *Genome Res.* **27**, 196 (2017).
27. L. Atia *et al.*, Geometric constraints during epithelial jamming. *Nat. Phys.* **14**, 613–620 (2018).
28. C. S. Chen, M. Mrksich, S. Huang, G. M. Whitesides, D. E. Ingber, Geometric control of cell life and death. *Science* **276**, 1425 (1997).
29. D. Bi, J. H. Lopez, J. M. Schwarz, M. L. Manning, A density-independent rigidity transition in biological tissues. *Nat. Phys.* **11**, 1074 (2015).
30. D. Bi, X. Yang, M. C. Marchetti, M. L. Manning, Motility-driven glass and jamming transitions in biological tissues. *Phys. Rev. X* **6**, 021011 (2016).
31. D. M. Sussman, M. Paoluzzi, M. C. Marchetti, M. L. Manning, Anomalous glassy dynamics in simple models of dense biological tissue. *EPL* **121**, 36001 (2018).
32. Y. W. Li, L. L. Y. Wei, M. Paoluzzi, M. P. Ciamarra, Softness, anomalous dynamics, and fractal-like energy landscape in model cell tissues. *Phys. Rev. E* **103**, 022607 (2021).
33. S. Sadhukhan, S. K. Nandi, Theory and simulation for equilibrium glassy dynamics in cellular potts model of confluent biological tissue. *Phys. Rev. E* **103**, 062403 (2021).
34. S. Sadhukhan *et al.*, Motility driven glassy dynamics in confluent epithelial monolayers. *Soft Matter* **20**, 6160 (2024).
35. R. Mandal, P. J. Bhuyan, P. Chaudhuri, C. Dasgupta, M. Rao, Extreme active matter at high densities. *Nat. Commun.* **11**, 2581 (2020).
36. R. Mandal, P. Sollich, Multiple types of aging in active glasses. *Phys. Rev. Lett.* **125**, 218001 (2020).
37. R. Wiese, K. Kroy, D. Levis, Fluid-glass-jamming rheology of soft active Brownian particles. *Phys. Rev. Lett.* **131**, 178302 (2023).
38. G. Szamel, E. Flenner, Extremely persistent dense active fluids. *Soft Matter* **20**, 5237 (2024).
39. S. Garcia *et al.*, Physics of active jamming during collective cellular motion in a monolayer. *Proc. Nat. Acad. Sci. U.S.A.* **112**, 15314–15319 (2015).
40. E. H. Zhou *et al.*, Universal behavior of the osmotically compressed cell and its analogy to the colloidal glass transition. *Proc. Nat. Acad. Sci. U.S.A.* **106**, 10632–10637 (2009).
41. B. R. Parry *et al.*, The bacterial cytoplasm has glass-like properties and is fluidized by metabolic activity. *Cell* **156**, 183–194 (2014).
42. K. Nishizawa *et al.*, Universal glass-forming behavior of in vitro and living cytoplasm. *Sci. Rep.* **7**, 15143 (2017).
43. N. Gravish, D. Monaenkova, M. A. D. Goodisman, D. I. Goldman, Climbing, falling, and jamming during ant locomotion in confined environments. *Proc. Natl. Acad. Sci. U.S.A.* **110**, 9746 (2013).
44. H. Lama, M. J. Yamamoto, Y. Furuta, T. Shimaya, K. A. Takeuchi, Emergence of bacterial glass. *PNAS Nexus* **3**, pgae238 (2024).
45. J. Deseigne, O. Dauchot, H. Chaté, Collective motion of vibrated polar disks. *Phys. Rev. Lett.* **105**, 098001 (2010).

46. P. Arora, A. K. Sood, R. Ganapathy, Motile topological defects hinder dynamical arrest in dense liquids of active ellipsoids. *Phys. Rev. Lett.* **128**, 178002 (2022).
47. J. Palacci, S. Sacanna, A. P. Steinberg, D. J. Pine, P. M. Chaikin, Living crystals of light-activated colloidal surfers. *Science* **339**, 936–940 (2013).
48. K. D. N. T. Lam, M. Schindler, O. Dauchot, Self-propelled hard disks: implicit alignment and transition to collective motion. *New J. Phys.* **17**, 113056 (2015).
49. B. Fabry *et al*., Scaling the microrheology of living cells. *Phys. Rev. Lett.* **87**, 148102 (2001).
50. G. Lenormand, J. Chopin, P. Bursac, J. J. Fredberg, J. P. Butler, Directional memory and caged dynamics in cytoskeletal remodelling. *Biochem. Biophys. Res. Commun.* **360**, 797 (2007).
51. L. Berthier, Nonequilibrium glassy dynamics of self-propelled hard disks. *Phys. Rev. Lett.* **112**, 220602 (2014).
52. R. Mandal, P. J. Bhuyan, M. Rao, C. Dasgupta, Active fluidization in dense glassy systems. *Soft Matter* **12**, 6268–6276 (2016).
53. R. Mandal, P. J. Bhuyan, P. Chaudhuri, M. Rao, C. Dasgupta, Glassy swirls of active dumbbells. *Phys. Rev. E* **96**, 042605 (2017).
54. E. Flenner, G. Szamel, L. Berthier, The nonequilibrium glassy dynamics of self-propelled particles. *Soft Matter* **12**, 7136–7149 (2016).
55. L. Berthier, E. Flenner, G. Szamel, How active forces influence nonequilibrium glass transitions. *New J. Phys.* **19**, 125006 (2017).
56. L. Berthier, G. Biroli, J. Bouchaud, R. L. Jack, *Dynamical Heterogeneities in Glasses, Colloids, and Granular Media* (Oxford University Press, 2011).
57. L. Berthier, J. Kurchan, Non-equilibrium glass transitions in driven and active matter. *Nat. Phys.* **9**, 310 (2013).
58. S. K. Nandi, N. S. Gov, Nonequilibrium mode-coupling theory for dense active systems of self-propelled particles. *Soft Matter* **13**, 7609–7616 (2017).
59. S. K. Nandi *et al*., A random first-order transition theory for an active glass. *Proc. Natl. Acad. Sci. U.S.A.* **115**, 7688–7693 (2018).
60. S. Dey, S. Karmakar, Scaling description of the relaxation dynamics and dynamical heterogeneity of an active glass-forming liquid. *Phys. Rev. E* **112**, 045420 (2025).
61. V. E. Debets, X. M. de Wit, L. M. C. Janssen, Cage length controls the nonmonotonic dynamics of active glassy matter. *Phys. Rev. Lett.* **127**, 278002 (2021).
62. M. C. Marchetti *et al*., Hydrodynamics of soft active matter. *Rev. Mod. Phys.* **85**, 1143–1189 (2013).
63. N. Klongvessa, F. Ginot, C. Ybert, C. Cottin-Bizonne, M. Leocmach, Active glass: Ergodicity breaking dramatically affects response to self-propulsion. *Phys. Rev. Lett.* **123**, 248004 (2019).
64. N. Klongvessa, C. Ybert, C. Cottin-Bizonne, T. Kawasaki, M. Leocmach, Aging or DEAD: Origin of the non-monotonic response to weak self-propulsion in active glasses. *J. Chem. Phys.* **156**, 154509 (2022).
65. G. Szamel, E. Flenner, L. Berthier, Glassy dynamics of athermal self-propelled particles: Computer simulations and a nonequilibrium microscopic theory. *Phys. Rev. E* **91**, 062304 (2015).
66. G. Szamel, Theory for the dynamics of dense systems of athermal self-propelled particles. *Phys. Rev. E* **93**, 012603 (2016).
67. M. Feng, Z. Hou, Mode coupling theory for nonequilibrium glassy dynamics of thermal self-propelled particles. *Soft Matter* **13**, 4464 (2017).
68. A. Liluashvili, J. Ónody, T. Voigtmann, Mode-coupling theory for active Brownian particles. *Phys. Rev. E* **96**, 062608 (2017).
69. K. Paul, A. Mutneja, S. K. Nandi, S. Karmakar, Dynamical heterogeneity in active glasses is inherently different from its equilibrium behavior. *Proc. Natl. Acad. Sci. U.S.A.* **120**, e2217073120 (2023).
70. V. E. Debets, C. Luo, S. Ciarella, L. M. C. Janssen, Generalized mode-coupling theory for mixtures of Brownian particles. *Phys. Rev. E* **104**, 065302 (2021).
71. V. E. Debets, L. M. C. Janssen, Mode-coupling theory for mixtures of athermal self-propelled particles. *J. Chem. Phys.* **159**, 014502 (2023).
72. S. Kolya, P. Pareek, S. K. Nandi, Active inhomogeneous mode-coupling theory (AIMCT) for dense systems of self-propelled particles. arXiv [Preprint] (2024). https://doi.org/10.48550/arXiv.2410.1592821 (Accessed 21 October 2025).
73. S. Pandey, S. Kolya, S. Sadhukhan, S. K. Nandi, The structure-dynamics feedback mechanism governs the glassy dynamics in epithelial monolayers. *Soft Matter* **21**, 269 (2025).
74. R. Mandal, S. K. Nandi, C. Dasgupta, P. Sollich, N. S. Gov, The random first-order transition theory of active glass in the high-activity regime. *J. Phys. Commun.* **6**, 115001 (2022).
75. L. Berthier, T. A. Witten, Compressing nearly hard sphere fluids increases glass fragility. *Europhys. Lett.* **86**, 10001 (2009).
76. L. Berthier, T. A. Witten, Glass transition of dense fluids of hard and compressible spheres. *Phys. Rev. E* **80**, 021502 (2009).
77. L. Berthier, E. Flenner, H. Jacquin, G. Szamel, Scaling of the glassy dynamics of soft repulsive particles: A mode-coupling approach. *Phys. Rev. E* **81**, 031505 (2010).
78. H. Jacquin, L. Berthier, F. Zamponi, Microscopic mean-field theory of the jamming transition. *Phys. Rev. Lett.* **106**, 135702 (2011).
79. M. Adhikari, S. Karmakar, S. Sastry, Dependence of the glass transition and jamming densities on spatial dimension. *Phys. Rev. Lett.* **131**, 168202 (2023).
80. E. Flenner, G. Szamel, Fundamental differences between glassy dynamics in two and three dimensions. *Nature Commun.* **6**, 7392 (2015).
81. V. E. Debets, L. M. C. Janssen, Active glassy dynamics is unaffected by the microscopic details of self-propulsion. *J. Chem. Phys.* **157**, 224902 (2022).
82. L. F. Cugliandolo, The effective temperature. *J. Phys. A Math. Theor.* **44**, 483001 (2011).
83. L. F. Cugliandolo, G. Gonnella, I. Petrelli, Effective temperature in active Brownian particles. *Fluc. Noise Lett.* **18**, 1940008 (2019).
84. I. Petrelli, L. F. Cugliandolo, G. Gonnella, A. Suma, Effective temperatures in inhomogeneous passive and active bidimensional Brownian particle systems. *Phys. Rev. E* **102**, 012609 (2020).
85. S. K. Nandi, N. S. Gov, Effective temperature of active fluids and sheared soft glassy materials. *Eur. Phys. J. E* **41**, 117 (2018).
86. G. Szamel, Self-propelled particle in an external potential: Existence of an effective temperature. *Phys. Rev. E* **90**, 012111 (2014).
87. D. Levis, L. Berthier, From single-particle to collective effective temperatures in an active fluid of self-propelled particles. *Europhys. Lett.* **111**, 60006 (2015).
88. R. Ni, M. A. C. Stuart, M. Dijkstra, Pushing the glass transition towards random close packing using self-propelled hard spheres. *Nat. Commun.* **4**, 2704 (2013).
89. A. Ikeda, L. Berthier, P. Sollich, Unified study of glass and jamming rheology in soft particle systems. *Phys. Rev. Lett.* **109**, 018301 (2012).
90. V. Lubchenko, P. G. Wolynes, Theory of structural glasses and supercooled liquids. *Annu. Rev. Phys. Chem.* **58**, 235–266 (2007).
91. T. R. Kirkpatrick, D. Thirumalai, Colloquium: Random first order transition theory concepts in biology and physics. *Rev. Mod. Phys.* **87**, 183–209 (2015).
92. A. Ikeda, L. Berthier, P. Sollich, Disentangling glass and jamming physics in the rheology of soft materials. *Soft Matter* **9**, 7669 (2013).
93. K. N. Pham *et al*., Multiple glassy states in a simple model system. *Science* **296**, 104–106 (2002).
94. S. K. Nandi, S. M. Bhattacharyya, S. Ramaswamy, Mode-coupling glass transition in a fluid confined by a periodic potential. *Phys. Rev. E* **84**, 061501 (2011).
95. S. Mandal *et al*., Multiple reentrant glass transitions in confined hard-sphere glasses. *Nat. Commun.* **5**, 4435 (2014).
96. S. Sadhukhan, C. Dasgupta, S. K. Nandi, Growing length and time scales in activity-mediated glassy dynamics in confluent cell monolayers. *Phys. Rev. E* **111**, 054416 (2025).
97. A. M. Philippe *et al*., Glass transition of soft colloids. *Phys. Rev. E* **97**, 040601 (2018).
98. J. Mattsson *et al*., Soft colloids make strong glasses. *Nature* **462**, 83–86 (2009).
99. M. Pelaez-Fernandez, A. Souslov, L. A. Lyon, P. M. Goldbart, A. Fernandez-Nieves, Impact of single-particle compressibility on the fluid-solid phase transition for ionic microgel suspensions. *Phys. Rev. Lett.* **114**, 098303 (2015).
100. R. Mandal, P. Sollich, How to study a persistent active glassy system. *J. Phys. Condens. Matter* **33**, 184001 (2021).
101. Y. E. Keta, R. Mandal, P. Sollich, R. L. Jack, L. Berthier, Intermittent relaxation and avalanches in extremely persistent active matter. *Soft Matter* **19**, 3871 (2023).
102. P. Arora *et al*., A shape-driven reentrant jamming transition in confluent monolayers of synthetic cell-mimics. *Nat. Commun.* **15**, 5645 (2024).